Integrated photonics on silicon with wide bandgap GaN semiconductor

N. Vico Triviño,[a] U. Dharanipathy, J.-F. Carlin, Z. Diao, R. Houdré, and N. Grandjean
Institute of Condensed Matter Physics, École Polytechnique Fédérale de Lausanne (EPFL), CH-1015 Lausanne, Switzerland

(Received 14 December 2012; accepted 15 February 2013; published online 1 March 2013)

We report on GaN self-supported photonic structures consisting in freestanding waveguides coupled to photonic crystal waveguides and cavities operating in the near-infrared. GaN layers were grown on Si (111) by metal organic vapor phase epitaxy. E-beam lithography and dry etching techniques were employed to pattern the GaN layer and undercut the substrate. The combination of low-absorption in the infrared range and improved etching profiles results in cavities with quality factors as high as ~5400. The compatibility with standard Si technology should enable the development of low cost photonic devices for optical communications combining wide-bandgap III-nitride semiconductors and silicon. © *2013 American Institute of Physics*. [http://dx.doi.org/10.1063/1.4793759]

The development of waveguides and photonic crystal (PhC) waveguides has been a topic of intense research effort during the past few years.[1–6] This is due to the broad application range from nano and micro-opto-electro-mechanical systems to classical and quantum telecommunications, thanks to the growing demand for more efficient and faster communication tools offering a reduced footprint. Most of conventional waveguides are fabricated on Si[1] using the so-called silicon-on-insulator (SOI) technology, which is well-established and presents a remarkable mechanical stability. However, it is intrinsically limited to passive devices owing to the indirect bandgap of Si. Waveguides based on direct bandgap III-V semiconductors such as GaAs[2] or InP[3,4] exhibit attractive features but at the expense of significant growth and fabrication effort.[7] In addition, InP presents a couple of issues like fragility, high temperature sensitivity, and relatively high cost. Thanks to their wide-bandgap, III-nitrides are potentially suitable for operation around 1.5 μm, although most of the past research focused on the visible spectral range. They offer low free carrier absorption[8] and negligible two-photon absorption.[9] They also exhibit a considerable mechanical hardness and a high thermal stability of the refractive index,[10] which is one order of magnitude larger than that of InP.[5,6] Furthermore, III-nitride epilayers have already been grown on silicon substrates with device quality, as shown by the fabrication of high-efficiency blue light emitting diodes.[11] Actually, GaN on silicon may offer a unique template for integrated photonics.[12,13]

However, besides the usual fabrication accuracy required for nanostructures such as PhCs, III-nitride-based materials suffer from several processing difficulties inherited from their intrinsic properties. For instance, etching vertical and smooth sidewalls is quite challenging owing to the hardness of GaN.

In addition, membranes are highly desirable in order to guarantee a refractive index contrast as high as possible between GaN and its cladding-like due to its low refractive index (~2.3 at 1.5 μm).[14] It is not required for SOI-based waveguides since the lower refractive index of SiO_2 compared to Si provides enough contrast to confine the light within the slab. The fabrication of freestanding III-nitride photonic structures by means of sacrificial layers has been reported by several groups using doping-selective and bandgap-selective photoelectrochemical etching and with different III-nitride sacrificial layers such as InGaN,[15] AlN,[16] and InAlN.[17] The main disadvantage of those approaches is the limited airgap thickness that can be achieved (only a few hundreds of nanometers). This might be particularly critical for structures operating in the near infrared.

Another approach consists in substrate underetching. To do so, heteroepitaxy is carried out on foreign substrates, which usually exhibit a large lattice-mismatch with GaN. This commonly leads to a high dislocation density (e.g., $>10^9\,cm^{-2}$ for GaN grown on Si).[18] The most common substrates used in III-nitride technology are SiC, Si, and sapphire. When considering substrate under-etching techniques, SiC and Si are excellent candidates since sapphire etching remains very challenging.[19,20] SiC offers a lower lattice mismatch with GaN (e.g., 3.5% for 6H-SiC (0001)) compared to Si (17% for Si (111)), but its cost is considerably larger. In addition, using Si is crucial for the forthcoming integration of photonics and electronics by taking advantage of both its low cost and well-established technology and the unique optoelectronic properties of III-nitrides. Indeed, in recent years, many efforts have been devoted to the integration of III-V semiconductors on Si platforms opening perspectives in silicon photonics (see Refs. 12, 13, and references therein). For instance, Pernice *et al.*[21] recently reported ultra-high quality factors (Q) in passive nanobeam cavities using AlN-on-SOI.

In this work, we report on the achievement of III-nitride-based freestanding waveguides and PhC cavities operating in the near infrared with Q factors of several thousands. These photonic structures are fabricated from GaN epilayers by underetching the Si (111) substrate.

The schematic of the whole photonic structure is shown in Fig. 1(a). It consists of fully suspended wire waveguides supported by tethers.[3,4] These tethered-waveguides are combined with so-called W1 PhC waveguides consisting in a missing row in a PhC lattice (triangular lattice with a filling factor of 0.3 and a lattice constant of 600 nm). Likewise, W1

[a]Author to whom correspondence should be addressed. E-mail: noelia.vicotrivino@epfl.ch.

 © 2013 American Institute of Physics

Downloaded 05 Mar 2013 to 128.178.175.77. Redistribution subject to AIP license or copyright; see http://apl.aip.org/about/rights_and_permissions

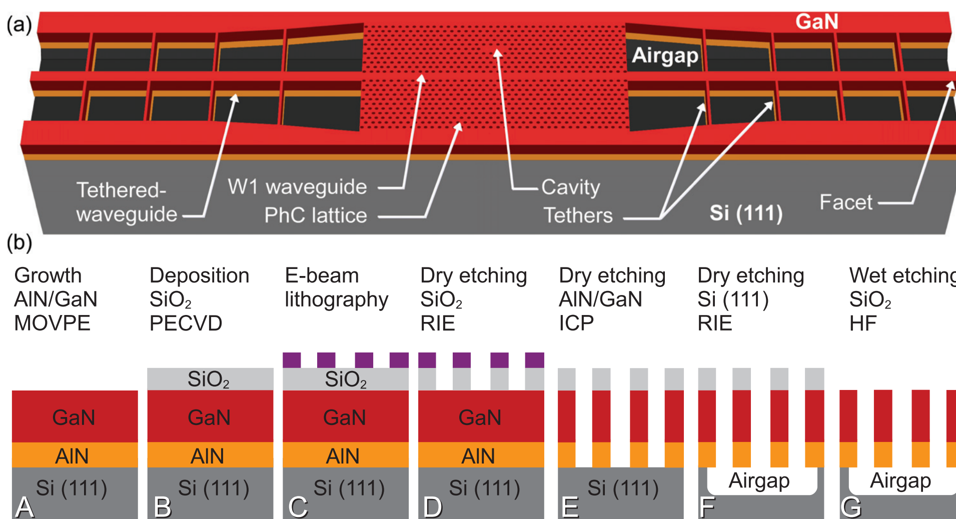

FIG. 1. (a) Schematic of the self-supported structure and (b) fabrication process flow.

waveguides are coupled to a PhC cavity. Different cavity designs were investigated that are discussed in this letter.

The fabrication process flow is summarized in Fig. 1(b). It starts with the growth of a thin (60 nm) AlN buffer layer on Si (111) followed by 330 nm of GaN along the *c*-axis (0001) by metal organic vapor phase epitaxy (A). The full width at half-maximum of the (0002) x-ray diffraction rocking curve is about 1800 arcsec, which is comparable with values from previous reports.[22] It is worth pointing out that such thin AlN/GaN layers grown on Si are affected by tensile strain mainly induced by the different thermal expansion coefficients. The total thickness was set to guarantee single optical mode operation. After the growth, a 100 nm thick SiO_2 layer was deposited on top of the epitaxial structure by plasma-enhanced chemical vapor deposition (B). This layer acts as a hard-mask during the whole fabrication process protecting the GaN surface and avoiding the degradation of the pattern. E-beam lithography was carried out to pattern the ZEP-520 A positive resist previously spun (C). Once the resist is developed, the pattern is transferred first to SiO_2 by fluorine-based reactive ion etching (RIE) (D) and then to the AlN/GaN stacked-layers using chlorine-based inductively coupled plasma etching (E). Finally, the membrane is released through dry fluorine-based RIE of the Si (111) substrate (F).[23,24] An airgap of the order of 3 μm was achieved, which is large enough to avoid light losses through the substrate at 1.5 μm. Finally, the SiO_2 layer was removed using a hydrofluoric acid solution (G). This is the most critical step due to the fragility of such self-supported structure, especially at the facets (see Fig. 1(a)), and very careful manipulation is required in order to prevent collapsing and peeling off of the wire waveguides. It is worth noticing that the whole structure, including the wire waveguides and PhC lattice, was fabricated in a single lithographic step, as well as in single subsequent etchings, which considerably reduces the time needed for the processing and simplifies it.

100 and 200 nm wide tethers were tested. It was found that the lower mechanical stability given by the narrower tethers results in collapsing, bending, and peeling-off of most of the waveguides. However, they offer lower scattering and, therefore, a compromise has to be found. In this first implementation, tethers were periodically spaced but forthcoming structures will feature a random distribution to avoid distributed Bragg reflector effect.[3] Likewise, two different cavities were investigated. First, the high-Q double-heterostructure (DH) proposed by Song *et al.*[25] based on a slight modulation of the lattice constant on a W1 waveguide was considered. Then, the well-known modified L3[26] cavity formed by three missing air holes and near-cavity holes shifted by 0.2 a was also realized. We point out that for both geometries, originally based on silicon parameters,[25,26] a complete redesign fully taking into account the refractive index of GaN has been performed. The orientation of the cavities and the waveguides is $[10\bar{1}0]$.

In Fig. 2, scanning electron microscope (SEM) and optical microscope images of the actual structures are displayed. In Fig. 2(a), a L3 cavity together with the W1 waveguide is shown. One can observe the high regularity of the PhC lattice. The smooth and vertical profiles of the holes sidewalls are shown in the inset of Fig. 2(a). Note that our process allowed us achieving a high verticality of the sidewalls ($< 5°$) with an aspect ratio of 3.[24] The pink-green contrast in the optical image (Fig. 2(b)) delimits the undercut areas (pink-like) and the 3 μm thick airgap is clearly evidenced in Fig. 2(c). Such large airgap confirms the high selectivity between III-nitrides and Si (111), which makes this fabrication process promising for the integration of III-nitrides on Si platforms.

Post-processing atomic force microscopy (AFM) measurements were performed on both the top (Figs. 3(a) and 3(b)) and back (Figs. 3(c) and 3(d)) sides of the processed structures. A slight trend for the holes toward a hexagonal shape can be seen, as previously observed in similar systems.[24,27] Concerning backside images, holes surprisingly look like bumps. This is an artifact related to the adhesive tape used for peeling-off and sticking the membrane to the sample holder. The adhesive material flows through the holes of the very thin membrane. The rms surface roughness of the W1 waveguide was measured for the top and back sides. It was found to be lower than 1.5 nm over a 500×500 nm^2 area in both cases. Figure 3(e) displays the surface roughness profile over 2 μm through the top (blue line) and back side (red-dashed line) of the W1 waveguide. The peak-valley height is lower than 2.5 nm.

Downloaded 05 Mar 2013 to 128.178.175.77. Redistribution subject to AIP license or copyright; see http://apl.aip.org/about/rights_and_permissions

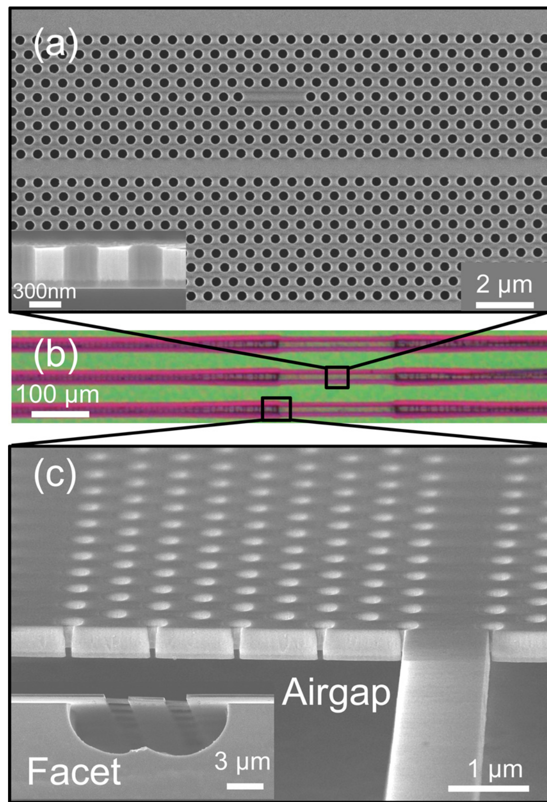

FIG. 2. (a) SEM top view of a L3 cavity together with a W1 waveguide. Inset: Cross-section of several holes. The roughness observed on the top layer comes from the SiO_2 hard mask, which was still not removed when the image was taken. (b) Optical microscope image of three of the structures. (c) SEM side view image (tilt of 20°) showing part of a wire waveguide, a W1 waveguide, and the PhC lattice. Inset: detail of one of the facets (tilt of −5°) exhibiting an airgap larger than 3 μm and several tethers supporting the suspended waveguide.

In order to validate the fabrication approach, an in-depth optical characterization of such structures was carried out.[28] The experimental setup consists of a standard end-fire configuration with a tunable laser diode operating around 1.5 μm with polarization control. A microlensed fiber is used to couple light into the facets and the light emitted from the top is collected by an objective with a numerical aperture of 0.90 to record real space image. That way, the propagation of infrared light through the W1 PhC waveguide for a wavelength above the light cone has been probed (Fig. 4). One can observe a large scattering arising from the tethers and especially from the intersection zone between the W1 PhC waveguide and the tethered-waveguide.

The W1 waveguide was used to couple light into the L3 (lateral coupling) and DH (in-line coupling with a barrier of ten periods (10a)) cavities. The emission peak of the DH (L3) cavity is centered at ∼1611 nm (∼1598 nm) and has a linewidth of ∼300 pm (∼730 pm).[28] Note that further adjustment of the wavelength to perfectly match the telecommunication window is straightforward by adapting the PhC lattice. The experimental Q factors are about equal to 2200 and 5400 for the L3 and DH cavities, respectively. The corresponding theoretical values, estimated by finite element simulations, are ∼2900 and ∼50 000, respectively. Given that all the structures were processed simultaneously, the larger difference between the theoretical and experimental values in the case of the DH cavities can be ascribed to two main factors. First, an infinite barrier was considered in the theoretical calculations instead of a finite one in the actual structure (10a). Second, a larger sensitivity of such cavities to hole position-accuracy is expected compared with its L3 counterpart. In the case of L3 cavities, the fact that both experimental and theoretical Q factor values are comparable is attributed to the low-defect fabrication process and to the relative long coupling distance between the W1 waveguide and the cavity (8 rows in this case). Indeed, a similar cavity placed only 6 rows away from the W1 waveguide exhibits a Q factor of ∼1900.

In summary, III-nitride-based freestanding waveguides and PhC cavities operating in the near-infrared have been investigated. The suspended wire waveguides are supported by tethers and coupled to W1 PhC waveguides. Both L3 and DH cavities have been fabricated exhibiting Q factors of ∼2200 and ∼5400, respectively. These results validate the

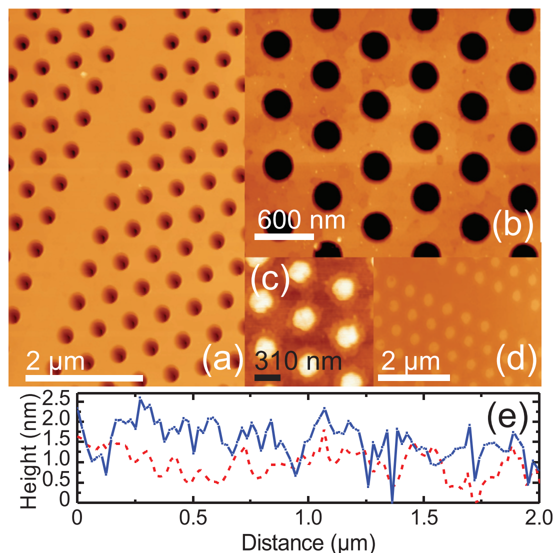

FIG. 3. (a) Top side AFM image of a W1 PhC waveguide. (b) Close-up view of the PhC lattice. (c) and (d) AFM images of the backside of (b) and (a), respectively. (e) Surface roughness profile of the W1 PhC waveguide taken from images (a) (blue line) and (d) (red-dashed line).

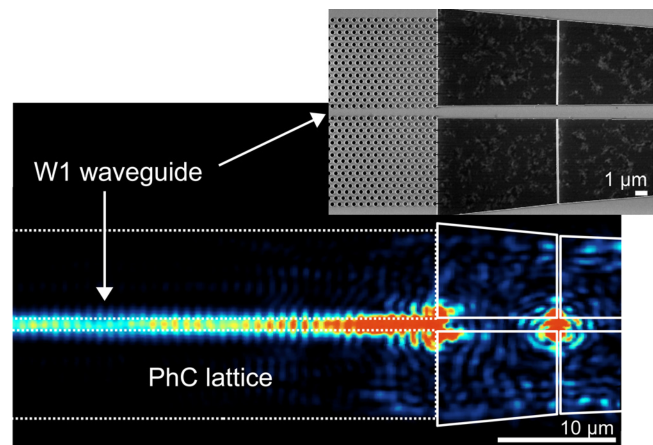

FIG. 4. Propagation of infrared light in a W1 waveguide for a wavelength above the light cone. Large scattering is observed at the location where the suspended wire and the W1 waveguide are coupled together and at the tethers location. Inset: SEM image of the corresponding structure (top view).

Downloaded 05 Mar 2013 to 128.178.175.77. Redistribution subject to AIP license or copyright; see http://apl.aip.org/about/rights_and_permissions

fabrication scheme employed here, which is fully compatible with standard Si technology. Such an approach can open promising routes toward the integration of both active and passive photonic components on the same wafer, minimizing both cost and size. In addition, the whole structure was obtained via a single lithographic step, which considerably reduces the processing time. Techniques such as nanoimprint lithography could be used to further minimize the cost. Hence, these results constitute a step forward in developing hybrid III-nitride/Si devices for integrated photonics.

The authors would like to thank R. Butté for fruitful discussions and a critical reading of the manuscript, Z. Benes for technical e-beam lithography advices, and N. Kaufmann for AFM measurements. This work was supported by the NCCR Quantum Photonics, research instrument of the Swiss National Science Foundation (SNSF) and by the SNSF (Grants Nos. 200020-113542 and 200020-140406).

[1]C. Jamois, R. B. Wehrspohn, L. C. Andreani, C. Hermann, O. Hess, and U. Gösele, Photonics Nanostruct. Fundam. Appl. **1**, 1 (2003).
[2]R. J. Deri and E. Kapon, IEEE J. Quantum Electron. **27**, 626 (1991).
[3]A. Talneau, K. H. Lee, S. Guilet, and I. Sagnes, Appl. Phys. Lett. **92**, 061105 (2008); A. Talneau, K. H. Lee, and I. Sagnes, IEEE Photon. Technol. Lett. **21**, 775 (2009).
[4]D. P. Kelly, M. W. Pruessner, K. Amarnath, M. Datta, S. Kanakaraju, L. C. Calhoun, and R. Ghodssi, IEEE Photon. Technol. Lett. **16**, 1298 (2004).
[5]R. Hui, S. Taherion, Y. Wan, J. Li, S. X. Jin, J. Y. Lin, and H. X. Jiang, Appl. Phys. Lett. **82**, 1326 (2003); R. Hui, Y. Wan, J. Li, S. X. Jin, J. Y. Lin, and H. X. Jiang, IEEE J. Quantum Electron. **41**, 100 (2005).
[6]A. Lupu, F. H. Julien, S. Golka, G. Pozzovivo, G. Strasser, E. Baumann, F. Giorgetta, D. Hofstetter, S. Nicolay, M. Mosca, E. Feltin, J.-F. Carlin, and N. Grandjean, IEEE Photon. Technol. Lett. **20**, 102 (2008).
[7]J. L. Pan, J. E. Mcmanis, T. Osadchy, L. Grober, J. M. Woodall, and P. J. Kindlmann, Nature Mater. **2**, 375 (2003).
[8]E. Kioupakis, P. Rinke, A. Schleife, F. Bechstedt, and C. G. Van de Walle, Phys. Rev. B **81**, 241201(R) (2010).
[9]C.-K. Sun, J.-C. Liang, J.-C. Wang, F.-J. Kao, S. Keller, M. P. Mack, U. Mishra, and S. P. DenBaars, Appl. Phys. Lett. **76**, 439 (2000).
[10]U. Tisch, B. Meyler, O. Katz, E. Finkman, and J. Salzman, J. Appl. Phys. **89**, 2676 (2001); N. Watanabe, T. Kimoto, and J. Suda, *ibid.* **104**, 106101 (2008).
[11]F. Reiher, A. Dadgar, J. Bläsing, M. Wieneke, M. Müller, A. Franke, L. Reißmann, J. Christen, and A. Krost, J. Phys. D: Appl. Phys. **42**, 055107 (2009).
[12]S. Lourdudoss, Curr. Opin. Solid State Mater. Sci. **16**, 91 (2012).
[13]T. Li, M. Mastro, and A. Dadgar, *III-V Compound Semiconductors: Integration with Silicon-Based Microelectronics* (CRC, New York, 2011).
[14]N. Antoine-Vincent, F. Natali, M. Mihailovic, A. Vasson, J. Leymarie, P. Disseix, D. Byrne, F. Semond, and J. Massies, J. Appl. Phys. **93**, 5222 (2003). The refractive index values were extrapolated to near-IR wavelengths by means of Sellmeier law.
[15]E. D. Haberer, R. Sharma, A. R. Stonas, S. Nakamura, S. P. DenBaars, and E. L. Hu, Appl. Phys. Lett. **85**, 762 (2004).
[16]J. R. Mileham, S. J. Pearton, C. R. Abernathy, J. D. MacKenzie, R. J. Shul, and S. P. Kilcoyne, Appl. Phys. Lett. **67**, 1119 (1995).
[17]J. Dorsaz, H.-J. Bühlmann, J.-F. Carlin, N. Grandjean, and M. Ilegems, Appl. Phys. Lett. **87**, 072102 (2005).
[18]E. Feltin, B. Beaumont, M. Laügt, P. de Mierry, P. Vennéguès, M. Leroux, and P. Gibart, Phys. Status Solidi A **188**, 531 (2001).
[19]V. Cimalla, J. Pezoldt, and O. Ambacher, J. Phys. D: Appl. Phys. **40**, 6386 (2007).
[20]Z. Yang, R. N. Wang, S. Jia, D. Wang, B. S. Zhang, K. M. Lau, and K. J. Chen, Phys. Status Solidi A **203**, 1712 (2006).
[21]W. H. P. Pernice, C. Xiong, C. Schuck, and H. X. Tang, Appl. Phys. Lett. **100**, 091105 (2012).
[22]H. Marchand, L. Zhao, N. Zhang, B. Moran, R. Coffie, U. K. Mishra, J. S. Speck, S. P. DenBaars, and J. A. Freitas, J. Appl. Phys. **89**, 7846 (2001).
[23]D. Néel, S. Sergent, M. Mexis, D. Sam-Giao, T. Guillet, C. Brimont, T. Bretagnon, F. Semond, B. Gayral, S. David, X. Checoury, and P. Boucaud, Appl. Phys. Lett. **98**, 261106 (2011).
[24]N. Vico Triviño, G. Rossbach, U. Dharanipathy, J. Levrat, A. Castiglia, J.-F. Carlin, K. A. Atlasov, R. Butté, R. Houdré, and N. Grandjean, Appl. Phys. Lett. **100**, 071103 (2012).
[25]B.-S. Song, S. Noda, T. Asano, and Y. Akahane, Nature Mater. **4**, 207 (2005).
[26]Y. Akahane, T. Asano, B.-S. Song, and S. Noda, Nature (London) **425**, 944 (2003).
[27]M. Arita, S. Ishida, S. Kako, S. Iwamoto, and Y. Arakawa, Appl. Phys. Lett. **91**, 051106 (2007).
[28]U. Dharanipathy, N. Vico Triviño, C. Yan, Z. Diao, J.-F. Carlin, N. Grandjean, and R. Houdré, Opt. Lett. **37**, 4588 (2012).

Downloaded 05 Mar 2013 to 128.178.175.77. Redistribution subject to AIP license or copyright; see http://apl.aip.org/about/rights_and_permissions